Progress of Theoretical Physics, Vol. 61, No. 4, April 1979

The Structure of ^{9}Be by a Molecular Model. II

Shigetō OKABE and Yasuhisa ABE*

Department of Physics, Hokkaido University, Sapporo 060
**Research Institute for Fundamental Physics, Kyoto University*
Kyoto 606

(Received October 28, 1978)

Motion of a valence neutron around two α-clusters is solved by the generator coordinate method with the effective nucleon-nucleon force which describes satisfactorily $\alpha+n$ and $\alpha+\alpha$ systems at low energies. It is shown that the wave functions obtained in the present calculation have two-center-like distributions and are well represented in terms of simple molecular orbitals, especially, in the ground rotational band. As for the positive parity states, additional components to the LCAO approximation are needed for quantitative discussion on the structure of a ^{9}Be nucleus. The motion is determined essentially by an effect of the Pauli principle between the valence neutron and a ^{8}Be core. Experimental energy levels are reproduced with a right binding energy from the ^{8}Be$+n$ threshold. Charge form factors for electron scattering to positive parity states are also reproduced as well as an r.m.s.-radius and a quadrupole moment of the ground state and charge form factors to members of the ground rotational band.

§ 1. Introduction

From molecular viewpoints various researches on light nuclei have been made in the last two decades. A number of states of the nuclei, especially $4N$-nuclei, have been comprehensively understood as a variety of modes of relative motion between clusters up to fairly high excitation energies.[1]

In order to study stability of α-cluster structure and motion of a valence nucleon in a clustering field we have recently investigated the ^{9}Be nucleus as a typical example by employing the molecular orbital model[2] which gives unified description of particle and molecule-like motion, and succeeded in reproducing an energy spectrum, electromagnetic properties of negative partity states and particle decay widths.[3),4)] We have shown that the α-cluster structure is persistent in the nucleus and that motion of a valence neutron is well represented in terms of the molecular orbitals. Moreover we have applied the model to the neighboring nuclei with a few valence nucleons which are weakly correlating with each other and are weakly bound in the field of a ^{8}Be core, and have explained large quadrupole moments and mass dependence of binding energies of boron isotopes.[5] However there remain some problems in the model. In the ^{9}Be nucleus the observed charge form factors for electron scattering to positive parity states, which are low-lying

anomalous parity states in the shell model version and often interpreted in weak-coupling models,[6] cannot be reproduced in the simple molecular orbital model (the LCAO approximation[3]). This indicates existence of missing components in the truncated space of the model.

As summarized in Ref. 3), many theoretical investigations have been carried out on the nucleus from different pictures, for example, the shell model and the cluster model.[7] Zahn has lately calculated the energy levels by employing the three-body resonating group method[8] and suggested that the positive parity states might be well described by the picture of two compressed α-clusters and an additional neutron. But none of theoretical attempt has given a satisfactory explanation for the problem of the charge form factors to the positive parity states.

The purposes of the present paper are to investigate the validity of the simple descriptions by the molecular orbitals and to resolve the problem in the positive parity states. For the purposes we solve motion of the valence neutron around two α-clusters by employing the generator coordinate method[9] and by using effective nucleon-nucleon force which describes satisfactorily $\alpha+n$ and $\alpha+\alpha$ systems at low energies. Motion of two α-clusters is determined as a result of a variational calculation for the total system with respect to a separation distance between the two α-clusters. Necessary expressions are given in § 2. In § 3 we discuss the validity of the LCAO approximation by the use of energy surfaces and of distributions of amplitudes of the valence neutron. In § 4 various properties of the ^{9}Be nucleus are well reproduced. The charge form factors to the positive parity states are shown to be reproduced excellently well. Conclusions are given in § 5.

§ 2. Generator coordinate method with molecular structure

We investigate motion of a valence neutron around two α-clusters under the following Hamiltonian with effective nucleon-nucleon force which gives good descriptions to the experimental data for $\alpha+n$ and $\alpha+\alpha$ systems at low energies.[10),11)]

$$H=T-T_{\rm cm}+V_{\rm c}+V_{\rm so}\,. \tag{1}$$

T is a sum of single-particle kinetic energy operators and $T_{\rm cm}$ a kinetic energy operator of the center-of-mass motion. The central force $V_{\rm c}$ consists of the Coulomb interaction and an effective central nucleon-nucleon interaction, for which we choose the Volkov potential:[12]

$$V_{\rm c}=\Sigma_{i<j}\left\{(1-m+mP^r_{ij})\cdot\Sigma_{k=1}^{2}V_k\exp\left(-\left(\frac{r_{ij}}{\mu_k}\right)^2\right)+\frac{1+\tau_z(i)}{2}\frac{1+\tau_z(j)}{2}\frac{e^2}{r_{ij}}\right\}, \tag{2}$$

where P^r_{ij} is the Majorana exchange operator and the strengths V_k are in MeV and the ranges μ_k in fm. The potential reproduces the experimental binding energies of ^{4}He and ^{16}O nuclei with the Majorana exchange mixture $m=0.60$. As the spin-orbit force $V_{\rm so}$ we adopt a semi-realistic two-body spin-orbit interaction in-

ferred from the study about effective interactions in nuclear matter by Nagata:[13]

$$V_{so}=\Sigma_{i<j}\boldsymbol{L}\cdot\boldsymbol{S}\cdot(0.5-0.5P^r_{ij})\,V_{LS}\left\{\exp\left(-\left(\frac{r_{ij}}{0.4472}\right)^2\right)-\exp\left(-\left(\frac{r_{ij}}{0.60}\right)^2\right)\right\}. \quad (3)$$

He has used the HN potential[14] for the central force and obtained a value of $V_{LS}=1200$ MeV. In this paper we take the Majorana exchange mixture of the central force and the strength of the spin-orbit force as adjustable parameters, and determined their values to give better fits to the experimental phase shifts of $\alpha+n$ and $\alpha+\alpha$ scattering at low energies by a microscopic treatment of scattering with a variational method proposed by Mito and Kamimura[15] (see Fig. 1). Values of parameters obtained are listed in Table I. Strengths of the spin-orbit force and of an odd state part of the central force have mutual dependence, because the parameters are determined for each state of the relative motion between nucleons. In spite of the same central force used, a value of the strength of the spin-orbit force differs from that used in the first paper, where a smaller value than a half of the present value was chosen. The choice was made to fit the experimental value of the splitting between the first $3/2^-$ and $1/2^-$ states in the truncated space of the molecular orbital model.

Using the Hamiltonian with the force *FI* or *FII* in Table I, we investigate the motion of the valence neutron around two α-clusters in extension of the molecular orbital model. Instead of using a linear combination of atomic orbitals, we employ a linear combination of wave packets of Gaussian form with a generator

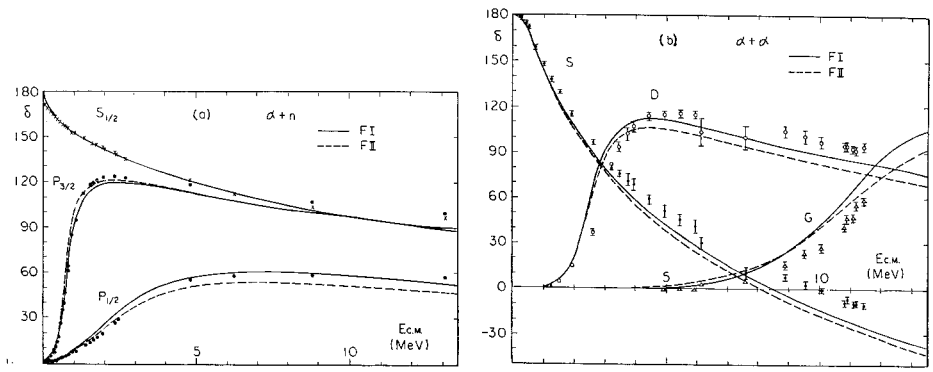

Fig. 1. Phase shifts (δ). (a) $\alpha+n$.[10] (b) $\alpha+\alpha$.[11]

Table I. Parameter sets.

	central force					spin-orbit force	size
	μ_1 (fm)	V_1 (MeV)	μ_2 (fm)	V_2 (MeV)	m	(V_{LS}) (MeV)	b (fm)
FI	1.60	−83.34	0.82	144.86	0.57	1600	1.41
FII	1.80	−60.65	1.01	61.14	0.60	2000	1.46

coordinate for the motion of the valence neutron. As generator coordinates, we take a separation distance between two α-clusters $S=|\boldsymbol{A}-\boldsymbol{B}|$ and a position vector directed from the two α-clusters to the center of the wave packet for the valence neutron $\boldsymbol{R}=\boldsymbol{C}-(\boldsymbol{A}+\boldsymbol{B})/2$ (Fig. 2). In actual calculations we treat one of the generator coordinates S as a variational parameter. The center-of-mass motion of the total system can be separated in the present treatment, because the center-of-mass motion of an α-cluster is also described by a wave packet of Gaussian form. The influence of zero-point oscillations of the two α-clusters on the motion of the valence neutron is expected to be small on the basis of the results of the previous paper.[3] The total variational wave function $\Psi_M^{J\pi}(S)$ is constructed from intrinsic states $\{\Phi(S\boldsymbol{R}\mu)\}$ which are Slater determinants belonging to the partition [441]:

$$\Psi_M^{J\pi}(S)=\Sigma_{K<0,\mu}\int d\boldsymbol{R}\, f_{K\mu}^{J\pi}(\boldsymbol{R})\cdot\Phi_{MK}^{J\pi}(S\boldsymbol{R}\mu), \tag{4}$$

$$\Phi_{MK}^{J\pi}(S\boldsymbol{R}\mu)=N_K^{J\pi}(S\boldsymbol{R}\mu)\cdot\hat{P}_{MK}^{J}\hat{P}^{\pi}\cdot\Phi(S\boldsymbol{R}\mu), \tag{5}$$

$$\langle\Psi_M^{J\pi}(S)\,|\,\Psi_M^{J\pi}(S)\rangle=\langle\Phi_{MK}^{J\pi}(S\boldsymbol{R}\mu)\,|\,\Phi_{MK}^{J\pi}(S\boldsymbol{R}\mu)\rangle=1, \tag{6}$$

$$\hat{P}_{MK}^{J}=\frac{2J+1}{8\pi^2}\int d\Omega\, D_{MK}^{J*}(\Omega)\hat{R}_{\Omega},\ \hat{P}^{\pi}=i^{(1-\pi)/2}(1+\pi\hat{P})/\sqrt{2}, \tag{7}$$

$$\Phi(S\boldsymbol{R}\mu)=\frac{1}{\sqrt{9!}}\det|0s0_{\boldsymbol{A}}{}^4\,0s0_{\boldsymbol{B}}{}^4\,0s0_{\boldsymbol{C}}\,\mu|, \tag{8}$$

$$|0s0_{\boldsymbol{A}}\rangle=(b^2\pi)^{-3/4}\exp\left(-(\boldsymbol{r}-\boldsymbol{A})^2/2b^2\right). \tag{9}$$

$\hat{P}_{MK}^{J}$ and $\hat{P}^{\pi}$ are projection operators for the total angular momentum J and the parity π, respectively. K is the projection along the symmetry axis of the total angular momentum, $N_K^{J\pi}(S\boldsymbol{R}\mu)$ a normalization constant, and μ a z-component of the spin of the valence neutron. Values of a size parameter $b=\sqrt{\hbar/(M\omega)}$ are determined from variational calculations for the ground state of the ^{9}Be nucleus and are listed in Table I together with force parameters.

Eigenvalues and weight functions $\{f_{K\mu}^{J\pi}(\boldsymbol{R})\}$ are determined by the Hill-Wheeler equation.[9] In practical calculations we use a finite linear combination of trial wave functions instead of an integral,

$$\Sigma_{K'>0,\mu',\boldsymbol{R}'}f_{K'\mu'}^{J\pi}(\boldsymbol{R}')\cdot\langle\Phi_{MK}^{J\pi}(S\boldsymbol{R}\mu)\,|H-E|\,\Phi_{MK'}^{J\pi}(S\boldsymbol{R}'\mu')\rangle=0. \tag{10}$$

As listed in Table II, fourteen configurations are chosen in the first quadrant of a (X,Z) plane of the generator coordinate $\boldsymbol{R}$ from the behavior of diagonal energy surfaces discussed in the next section. K and μ are restricted within $K_L^{\pi}(K_L=K-\mu)\leq 2^+,\ 3^-$.

§ 3. Validity of the LCAO approximation

In order to discuss the motion of the valence neutron we first calculate energy

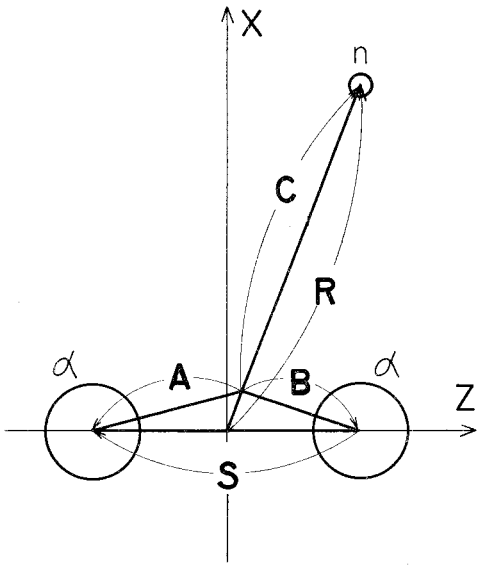

Fig. 2. Schematic diagram of $2\alpha+n$ and generator coordinates. $\boldsymbol{A}$, $\boldsymbol{B}$ and $\boldsymbol{C}$ are position vectors to the centers of the wave packets for two α-clusters and a valence neutron, respectively. ($\boldsymbol{A}+\boldsymbol{B}+\boldsymbol{C}=0$.)

Table II. Mesh points.

	R_x(fm)	R_z(fm)
1	0.0	0.0
2	0.0	3.0
3	0.0	5.0
4	2.0	0.0
5	4.0	0.0
6	6.0	0.0
7	1.0	1.75
8	2.5	1.75
9	4.0	2.0
10	5.5	2.5
11	1.5	3.5
12	3.0	4.0
13	4.5	4.5
14	2.0	5.5

case 1 7, 8, 9, 10
case 2 1, 2, 11, 12, 13
case 3 All

surfaces which are given by diagonal energy matrix elements in Eq. (10) with respect to various values of the generator coordinate $\boldsymbol{R}$ in Fig. 2 for the motion of the valence neutron. It is worth noticing here that in the limit when $\boldsymbol{C}$ approaches $\boldsymbol{B}$, a wave function of the valence neutron ϕ goes to that of the LCAO approximation due to an orthogonality to single-particle states which are occupied by nucleons in the α-clusters, for example,

$$(1)\quad K^\pi=1^- \quad \phi\sim|0p1_{\boldsymbol{A}}+0p1_{\boldsymbol{B}}\rangle \quad \text{for} \quad C_x\to 0 \quad \text{and} \quad C_z=B_z\,, \tag{11}$$

$$(2)\quad K^\pi=0^+ \quad \phi\sim(1-|0s0_{\boldsymbol{A}}+0s0_{\boldsymbol{B}}\rangle\langle 0s0_{\boldsymbol{A}}+0s0_{\boldsymbol{B}}|)\,|0p0_{\boldsymbol{A}}-0p0_{\boldsymbol{B}}\rangle \quad \text{for} \quad C_x=0 \quad \text{and} \quad C_z\to B_z\,, \tag{12}$$

where $|nlm_{\boldsymbol{A}}\rangle$ is an eigenfunction of a three-dimensional harmonic oscillator around a point $\boldsymbol{A}$ in the spherical coordinate. This means that the present treatment has a wider functional space for describing the valence neutron than the LCAO approximation. Thus we can investigate the validity of the LCAO approximation. We take up the ground $3/2^-$ state and the first excited $1/2^+$ state at 1.68 MeV, since they are typical and basic states in structure of the ^{9}Be nucleus. For the purpose of comparison we also calculate energy surfaces with the $SU(3)$ shell model wave function of the ^{8}Be core which is approximately given by the cluster wave function in the limit of a small S/b.

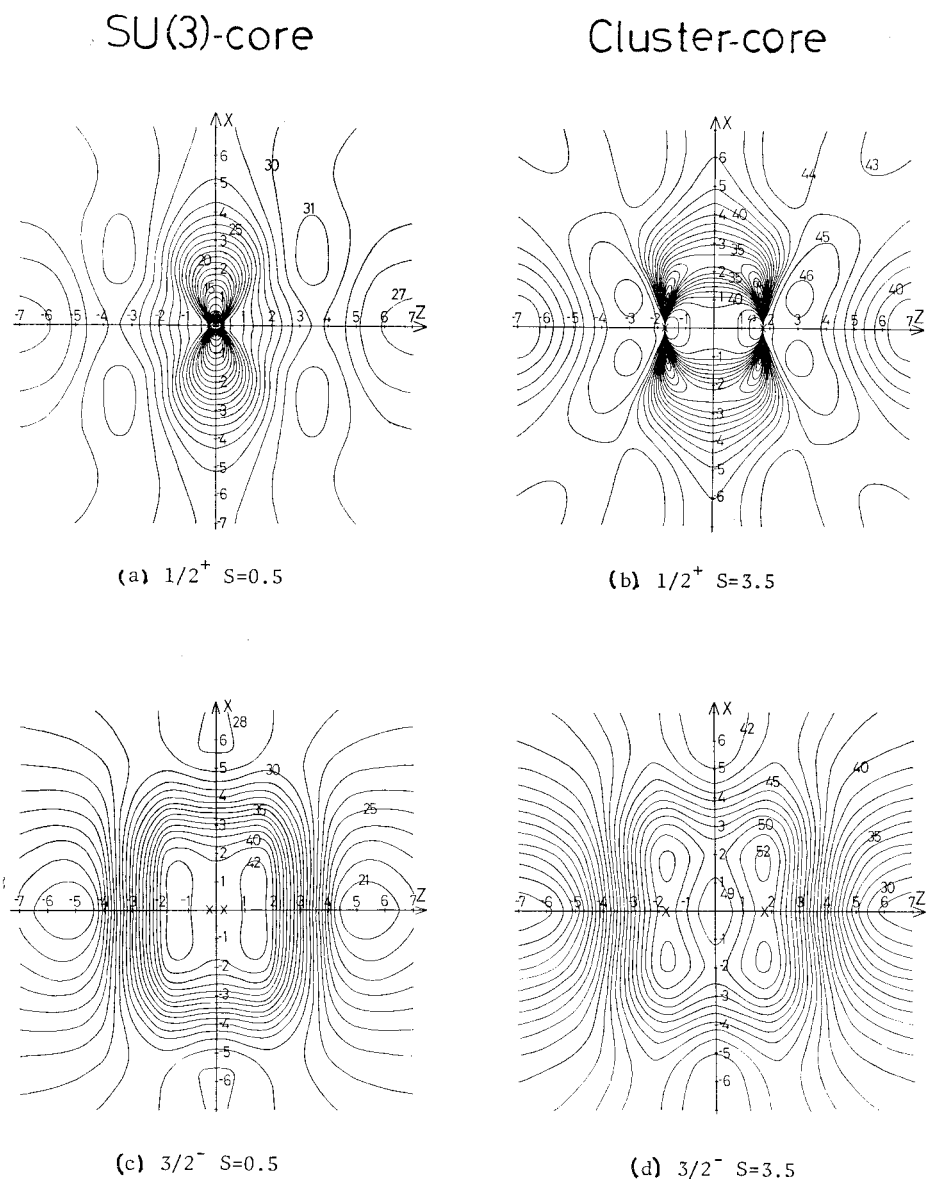

Fig. 3. Conotur maps of the total binding energy in MeV with *FI*. Mark × denotes a position of α-particle.

Contour maps of the total binding energy with the force *FI* are shown in Fig. 3 for $J^{\pi}=3/2^{-}$ $(K=3/2, K_L=1)$ and $1/2^{+}$ $(K=1/2, K_L=0)$ in a coordinate system of the valence neutron (Fig. 2) with the fixed values of a separation distance between two α-clusters, $S=0.5$ (the shell configuration of the ^{8}Be core) and $S=3.5$ (the cluster configuration) which is an energy minimum point for the

^{8}Be nucleus. As the basis vector is an eigenstate of the total angular momentum and the parity, each figure is symmetry with respect to the X and Z axes. Contour lines with large numerals correspond to energy valleys, while those with small numerals to energy barriers or ridges. As a whole, energy surfaces are polarized, that is, valleys in the maps for the $3/2^-$ state and the $1/2^+$ state are polarized along directions of the X-axis and the Z-axis respectively, in both the shell and the cluster configurations of the ^{8}Be core. Patterns of the contour maps for the $1/2^+$ state ((a) and (b) in Fig. 3) are very different between the shell and the cluster configurations, while those for the $3/2^-$ state are rather similar.

Next we solve the motion of the valence neutron in the case of the cluster configuration of the ^{8}Be core. It is apparent from the contour maps ((b) and (d) in Fig. 3) that important mesh points for the $3/2^-$ state are different from those for the $1/2^+$ state. A set of case 1 in Table II is that for the $3/2^-$ state and a set of case 2 for the $1/2^+$ state. In the final solution we use the set of case 3 which includes more mesh points than the sum of them. Overlappings between wave functions obtained in the present model and the LCAO approximation with the same parameters (FI, $S=3.5$ fm) are shown in Table III, where we list up the states whose overlapping on one of the states in the LCAO approximation is above 0.50. Moreover, we have calculated a "*two-dimensional reduced width amplitude* $|Z^{J\pi}_{K\mu}(\boldsymbol{a})|_{a_y=0}$" of the valence neutron with $S=3.5$ fm in order to see distributions of the valence neutron intuitively.

$$Z^{J\pi}_{K\mu}(\boldsymbol{a}) = \sqrt{\binom{9}{1}}\langle \Psi^{J\pi}_M(S)\,|\,N^{J\pi}_{K\mu}(\hat{\boldsymbol{a}})\,\hat{P}^J_{MK}\hat{P}^\pi\,|\,\Phi(S;\,^8\mathrm{Be})\cdot\delta(\boldsymbol{r}-\boldsymbol{a}),\,\mu\rangle\,, \tag{13}$$

$$\Phi(S;\,^8\mathrm{Be}) = \frac{1}{\sqrt{8!}}\det|0s0_{\boldsymbol{A}}{}^4\,0s0_{\boldsymbol{B}}{}^4|, \tag{14}$$

$$(1/N^{J\pi}_{K\mu}(\hat{\boldsymbol{a}}))^2 = \langle \hat{P}^J_{MK}\hat{P}^\pi(\Phi(S;\,^8\mathrm{Be})\,\delta(\hat{\boldsymbol{r}}-\hat{\boldsymbol{a}})\,\mu)\,|\,\hat{P}^J_{MK}\hat{P}^\pi(\Phi(S;\,^8\mathrm{Be})\,\delta(\hat{\boldsymbol{r}}-\hat{\boldsymbol{a}})\,\mu)\rangle\,, \tag{15}$$

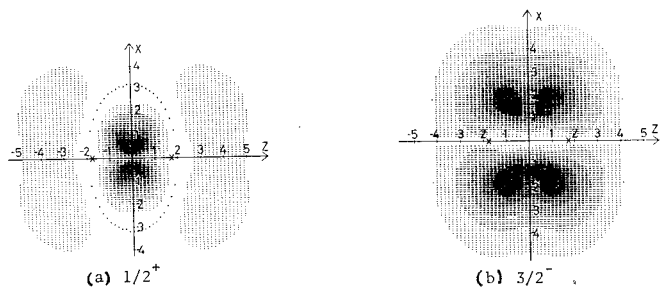

Fig. 4. Two-dimensional reduced the amplitude $|Z^{J\pi}_{K\mu}(\boldsymbol{a})|_{a_y=0}$. (a) $1/2^+$ ($K=1/2$, $\mu=1/2$). (b) $3/2^-$ ($K=3/2$, $\mu=1/2$).

Table III. Overlappings between the present model ($2\alpha+n$) and the LCAO model.[3]

$2\alpha+n$ \ LCAO	1st	2nd	3rd	$2\alpha+n$ \ LCAO	1st	2nd	3rd
$1/2_1^+$	0.805	0.014	—	$1/2_3^-$	0.105	−0.596	—
$1/2_3^+$	0.049	−0.506	—	$3/2_1^-$	−0.936	0.019	−0.022
$3/2_1^+$	−0.781	−0.002	0.041	$3/2_2^-$	0.026	−0.827	−0.036
$3/2_3^+$	−0.142	0.563	0.278	$5/2_1^-$	0.926	0.025	0.007
$5/2^+$	−0.884	−0.005	0.021	$5/2_2^-$	0.041	0.762	0.125
$7/2_1^+$	0.737	−0.051	0.060	$7/2_1^-$	0.883	0.000	0.091
$7/2_2^+$	0.281	0.049	−0.503	$7/2_2^-$	0.290	−0.511	−0.231
$9/2^+$	0.874	0.028	−0.029	$7/2_3^-$	0.123	0.509	−0.022
$1/2_1^-$	−0.832	−0.041	—	$9/2^-$	−0.906	0.019	−0.005

where $\boldsymbol{r}$ and $\hat{\boldsymbol{r}}$ are a coordinate of the valence neutron and its angular part, respectively. $|Z^{J^\pi}_{K\mu}(\boldsymbol{a})|_{a_y=0}$ is drawn in Fig. 4.

As for the $3/2^-$ state, the energy valley in Fig. 3 is deep and localized. An overlapping between the present solution and the basis wave function at the energy minimum point $\langle \Psi_M^{J^\pi}(S) | \Phi_M^{J^\pi}(S, (R_x, R_z) = (1.5, 1.75), K=3/2, K_L=1) \rangle_{J^\pi=3/2^-, S=3.5}$ is very large and is 0.959, which shows that there exists stable intrinsic state for the ground rotational band. The map d in the Figure strongly resembles a density distribution of a wave function of the valence neutron in the LCAO approximation which has its maxima just above and below the positions of the α-clusters in parallel to the X-axis. Actually the amplitude $|Z^{J^\pi}_{K\mu}(\boldsymbol{a})|_{a_y=0}$ obtained for the state has nodal points ($Z^{J^\pi}_{K\mu}(\boldsymbol{a})=0.$) along a Z-axis and shows two-center-like distribution. As expected, a value of the overlapping between the present solution and the LCAO wave function in the $3/2^-$ state is large (-0.936). The overlappings in the other members of the ground rotational band are also large and are 0.926, 0.883, -0.906 for the $5/2_1^-$, $7/2_1^-$, $9/2_1^-$ states respectively. As for the rotational band with $K^\pi=1/2^-$, the overlappings are somewhat reduced. The differences between $K^\pi=3/2^-$ and $1/2^-$ rotational bands are understood by an effect of the spin-orbit force. It brings the $3/2^-$ state close to the limit of the LCAO approximation, while it spreads the wave

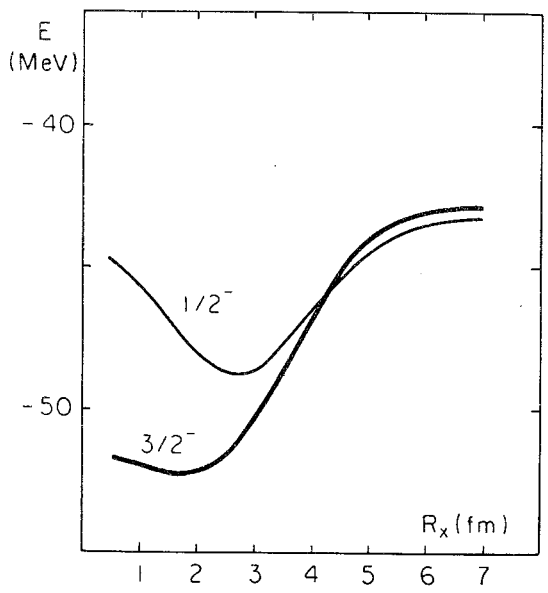

Fig. 5. The total energy curves with FI vs R_x (R_z =1.75 fm) for $3/2^-$ ($K=3/2$, $K_L=1$) and $1/2^-$ ($K=1/2$, $K_L=1$).

function of the $1/2^-$ state a little, as shown in Fig. 5.

The map of the $1/2^+$ state ((b) in Fig. 3) is quite different from that of the $3/2^-$ state ((d) in Fig. 3), characterized by remarkably high barriers, which depend on positions of two α-clusters, and the valley is shallow and spreads over the outer region. It, however, is rather similar to the density distribution of a wave function of the valence neutron in the LCAO approximation, which has maxima on Z-axis and nodes just at the positions of two α-clusters. The apparent difference is that the maxima are pushed aside a little from the Z-axis. This situation is also seen from the amplitude $|Z^{J^\pi}_{K\mu}(\boldsymbol{a})|_{a_y=0}$ obtained for the $1/2^+$ state in Fig. 4(a), which has nodal points along a dotted line like a spherical $1s$ orbital but shows large polarized distribution like the LCAO wave function. Here, we take up a ratio of the spectroscopic factor $S^{J^\pi}_{Ll_j}$ for $^8\mathrm{Be}+n$ channels discussed in the next section, from which we can obtain the information about an overlapping between the present solution and the weak-coupling limit. The ratio $S^{1/2^+}(0^+(^8\mathrm{Be})\otimes s_{1/2}(n))$: $S^{1/2^+}(2^+(^8\mathrm{Be})\otimes d_{3/2}(n))$: $S^{1/2^+}(2^+(^8\mathrm{Be})\otimes d_{5/2}(n))$ is 0.79: 0.04: 0.30 for the present solution, while it is 0.59: 0.09: 0.53 for the LCAO wave function. On the other hand, the overlapping between the present solution and the basis wave function at the energy minimum point $\langle \Psi_M^{J^\pi}(S)\,|\,\Phi_M^{J^\pi}(S, (R_x, R_z)=(1.0, 3.0), K=1/2, K_L=0)\rangle_{J^\pi=1/2^+, S=3.5}$ is not small (0.869). These facts mean that the $1/2^+$ state has an intermediate character between the weak- and strong-coupling limit. As for the other positive parity states, $3/2^+$ and $7/2^+$ states are more close to the weak-coupling limit, while $5/2^+$ and $9/2^+$ states are close to the limit of the LCAO approximation in almost the same extent as the members of the ground rotational band. This difference is caused by the effect of the spin-orbit force. Even in the positive parity states, the valence neutron does not move freely around the ^{8}Be core, but its motion is confined rather strongly.

Finally we discuss a reason why such a confinement happens to the motion of the valence neutron in the ^{9}Be nucleus. As is seen in the contour maps (b) and (d) in Fig. 3, the confinements are generated essentially by the existence of the barriers or the ridges in both the $3/2^-$ and the $1/2^+$ state. In the case of the $3/2^-$ state there are the rising barriers to $|Z|$-directions and the ridge on the Z-axis due to the existence of two α-clusters on the Z-axis, and in the case of the $1/2^+$ state there is the combined ridge which is extremely high at the positions of two α-clusters on the Z-axis. As is recognized intuitively, they all come from the Pauli exclusion principle between the valence neutron and the nucleons in the ^{8}Be core with two α-cluster configuration. The rising ridge to $|Z|$-direction in the $3/2^-$ state means nothing but the fact that the single-particle state which extends along Z-axis is already occupied by the nucleons in the α-clusters. The extremely high ridge in the $1/2^+$ state is just a reflection of the fact that the valence neutron cannot get into the α-clusters. In fact, in the limit when $\boldsymbol{C}$ approaches $\boldsymbol{B}$ as $C_x\to 0$ with $C_z=B_z$,

$$\phi\sim\phi(200;\boldsymbol{B}), \tag{16}$$

and as $C_z \to B_z$ with $C_x = 0$,

$$\phi \sim \phi(001; \boldsymbol{B}), \tag{17}$$

where $\phi(n_x n_y n_z; \boldsymbol{B})$ denotes a wave function of the valence neutron around the point $\boldsymbol{B}$ and n_x, n_y and n_z are quantum numbers of one-dimensional harmonic oscillators.

§ 4. Structure of ^{9}Be nucleus

Since it has turned out in § 3 that the motion of the valence neutron is well represented in the LCAO approximation, especially, for the ground rotational band, we expect that such properties as is satisfactorily explained in the previous paper, for example, an energy spectrum and charge form factors of the ground rotational band, will be reproduced in the present treatment as well. However in the LCAO approximation we have failed in reproducing the charge form factors to positive parity states. In this section we discuss structure of the ^{9}Be nucleus including the above form factors in the present framework of the generator coordinate method for the motion of the valence neutron.

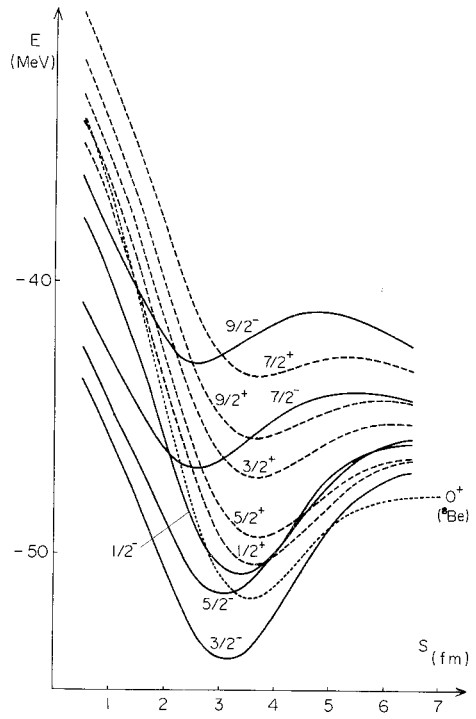

Fig. 6. The total energy curves with *FI* vs separation distance S. Solid line: negative parity states. Dashed line: positive parity states. Dotted line: ^{8}Be(0^+) with $b = 1.37$ fm (a variational value).

We first carry out variational calculations with respect to the separation distance S, from which we are able to know changes of the ^{8}Be core by an additional neutron. As shown in Fig. 6, the present results with the force *FI* have almost the same bahaviors as those of the previous paper. The ground rotational band has a tendency of the anti-stretching, while values of the minimum points for the positive parity states are almost independent on the states and are close to that of the ^{8}Be nucleus, which suggests that the neutron may be weakly bound with the ^{8}Be core in the positive parity states.

We calculate energy spectra using an optimum value S for each angular momentum state. As is shown in Fig. 7, the present calculation reproduces the observed energy spectra with a right binding energy from a threshold of $^8\mathrm{Be} + n$.

Energy levels of the $3/2^-$, $1/2^-$ and $1/2^+$ rotational bands are predicted as well as in the LCAO approximation. We have many quasi-bound states at high excitation energies due to the bound state approximation. Although the states must be examined under the scattering boundary condition, the third $3/2^+$ state is expected to exist acutually among them, because it has a large overlapping on the state in the LCAO approximation (see Table III) and has structure of a partner of a parity inversion doublet with the ground $3/2^-$ state and may be a candidate for the Pygmy resonance in a photo-neutron reaction.[16] As for a dependence on effective force, *FII* is slightly repulsive than *FI* in the nucleus, while they give almost the same results for the $\alpha+n$ and $\alpha+\alpha$ systems. We compare energy levels in the cluster configuration of the ^{8}Be core with those in the shell configuration, by using the same force *FI*. In the latter we use a value of the size parameter $b=1.70$ fm so as to give a reasonable value to an r.m.s.-radius. With such a larger value of b we can reproduce the experimental value of the spin-orbit splitting between the first $3/2^-$ and $1/2^-$ states. As shown in Fig. 8, the positive parity states are still high lying in the shell configuration. As another remarkable difference between the shell and cluster configuration of the ^{8}Be core, it should be stressed here that the $3/2^-$ and $5/2^-$ members of the $1/2^-$ rotational band exist closely with each other in the former configuration, while they behave themselves like a rigid rotor in the latter, as discussed in the previous paper.

The r.m.s.-radius $\langle r^2\rangle^{1/2}$ of the ground state is determined from the elastic charge form factors and is recently deduced to be 2.46 ± 0.11 fm.[7] The quadrupole

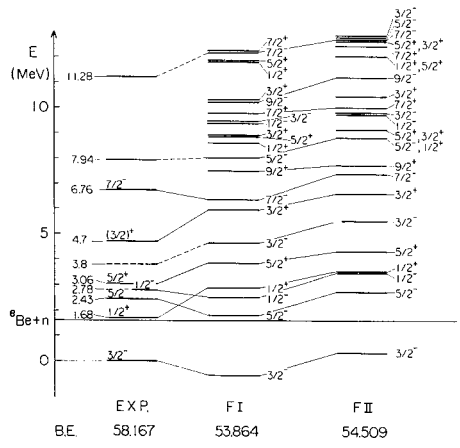

Fig. 7. Energy spectra from ^{8}Be$+n$ threshold. B.E. denotes the total binding energy.

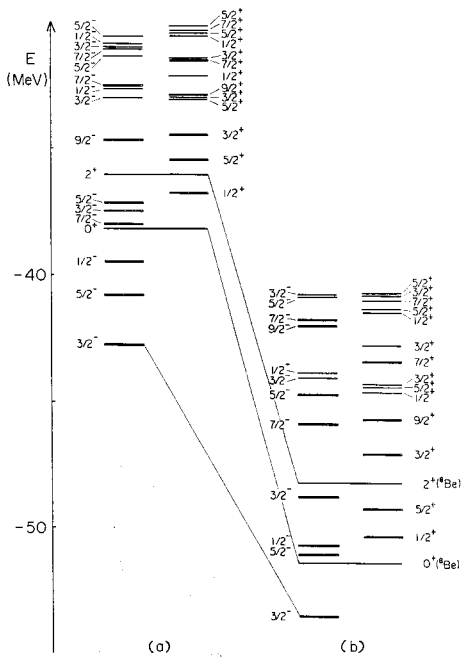

Fig. 8. Comparison of energy spectra with *FI* between shell configuration ((a) $S=0.5$ fm, $b=1.7$ fm) and cluster configuration ((b) $S=3.5$ fm, $b=1.41$ fm).

moment Q of the ground state is determined from several experimental methods and are deduced to be in between $+3.0$ and $+6.5\,\mathrm{fm}^2$.[7] Calculated values are $\langle r^2\rangle^{1/2}=2.43\,\mathrm{fm}$, $Q=+4.58\,\mathrm{fm}^2$ with *FI* and $\langle r^2\rangle^{1/2}=2{,}53\,\mathrm{fm}$, $Q=+5.10\,\mathrm{fm}^2$ with *FII*, and are almost the same as those in the LCAO approximation.

We carry out calculations of charge form factors for electron scattering,

$$|F(q^2)|^2_{i\to f}=\frac{1}{Z^2(2J_i+1)}\Sigma_{M_iM_f}|\langle J_fM_f|\Sigma_j\frac{1+\tau_z(j)}{2}\,e^{i\boldsymbol{q}\boldsymbol{r}_j}|J_iM_i\rangle|^2. \qquad (18)$$

The correction for the center-of-mass motion is made exactly and that for the finite proton size is made in the same way as the previous paper with a Gaussian form factor. As is shown in Fig. 9, the present calculations reproduce the charge form factors to members of the ground rotational band as well as the LCAO approximation did. The charge form factors calculated with *FII* give better fits to the experiments,[17)~21)] which is due to the fact that wave functions obtained with *FII* have larger clustering ($S_{\min}(3/2^-)=3.3\,\mathrm{fm}$) than those with *FI* ($S_{\min}(3/2^-)=3.1\,\mathrm{fm}$).

Next we discuss the charge form factors to the positive parity states. As shown in Fig. 10, the charge form factor to the $1/2^+$ state at 1.68 MeV[21),22)] has been found to be reproduced excellently well, which has never been achieved in any

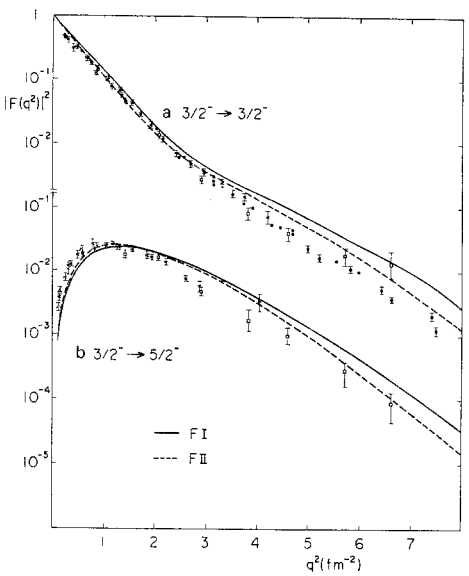

Fig. 9. Charge form factors to the ground rotational band. a: elastic form factors.[17)~19)] b: inelastic form factors to the $5/2^-$ state at 2.43 MeV.[18),20),21)]

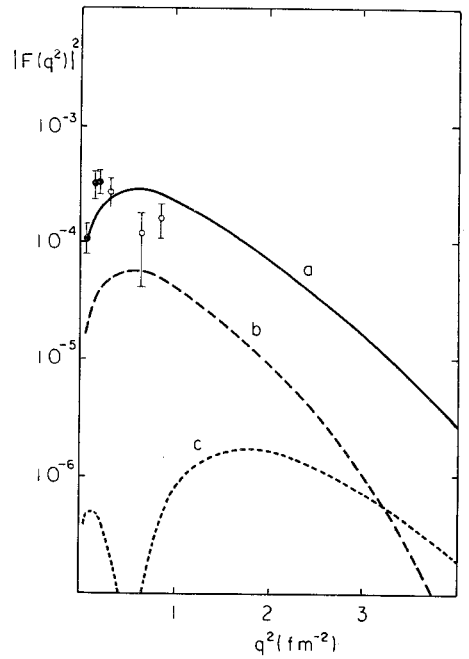

Fig. 10. Inelastic charge form factors to the $1/2^+$ state at 1.68 MeV.[21),22)] a: final result. b: one-point approximation. c: LCAO approximation.

models. The difference of the calculated form factors between the present model and the LCAO approximation is very striking, which is seen in comparison of curve a and c in Fig. 10. If we take basis vectors at energy minimum points for the ground $3/2^-$ state and the $1/2^+$ state, we have completely different dependence on transfer momenta from that in the LCAO approximation, with fairly large magnitude (curve b from curve c in Fig. 10). This is caused by small components not included in the LCAO approximation. These components come from the configuration at the minimum points for the $1/2^+$ state, which are located a little apart from the Z-axis (see (b) in Fig. 3). Furthermore "zero-point oscillation" around the minima makes magnitude of the form factors larger and gives excellent fits to the experiments. As is shown in Fig. 11, the charge form factor to the $5/2^+$ state at 3.06 MeV[22] are also improved in the present calculation. The experimental data on the charge form factors to the positive parity states at high transfer momenta are strongly desired.

Finally we calculate neutron reduced width amplitudes for the ground $3/2^-$ state and the $1/2^+$ state:

$$\mathcal{Y}^{J^\pi}_{(Lij)}(a)=\sqrt{\binom{9}{1}}\left\langle \Psi^{J^\pi}_M(S)\left|\left[\Phi(S;{}^8\mathrm{Be})\otimes\left[\frac{1}{r^2}\delta(r-a)Y_l(\hat{\boldsymbol{r}})\otimes\theta_{1/2}\right]_j\right]_{JM}\Phi_G\right\rangle, \quad (19)$$

where Φ_G is a wave function of the center-of-mass motion and $\theta_{1/2}$ is a spin wave

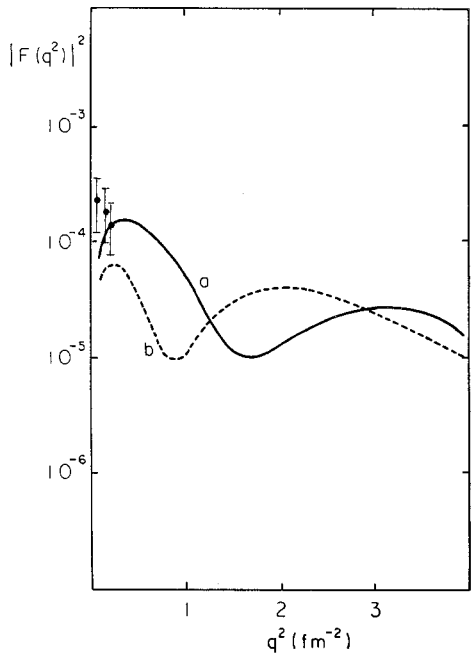

Fig. 11. Inelastic charge form factors to the $5/2^+$ state at 3.06 MeV.[22] a: final result. b: LCAO approximation.

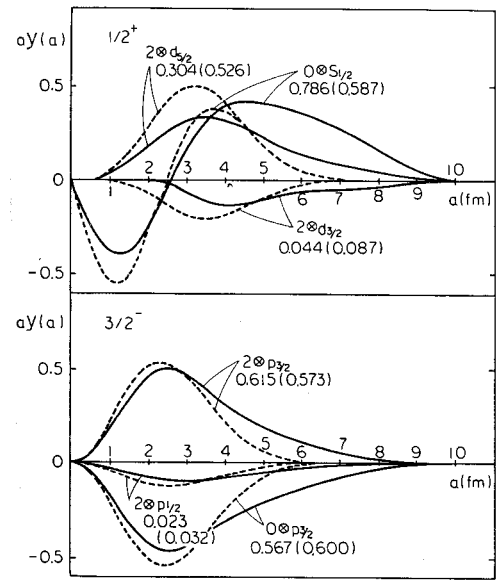

Fig. 12. Neutron reduced width amplitudes ($\mathcal{Y}^{J^\pi}_{Lij}(a)$) for $[L(^8\mathrm{Be})\otimes[l\otimes 1/2]_j(n)]_{JM}$ channels. Numerals in figures are values of spectroscopic factor $S^{J^\pi}_{Lij}$ and numerals in parentheses are values of $S^{J^\pi}_{Lij}$ in the LCAO approximation (the same force and $S_{\min}$ are used).

function. A spectroscopic factor $S^{J^\pi}_{Ll_j}$ is defined as

$$S^{J^\pi}_{Ll_j}=\int_0^\infty da\,|a\mathcal{Y}^{J^\pi}_{(Ll_j)}(a)|^2. \tag{20}$$

As is seen in Fig. 12 the behaviors of the tail parts of the amplitudes obtained in the calculation (solid line) are improved in comparison with those of the previous LCAO approximation (dashed line). The improvement corresponds to the change in the charge form factor (from curve b to curve a in Fig. 10). A value of the spectroscopic factor for each channel in the $3/2^-$ state is almost the same as the value in the LCAO approximation. On the contrary, the values of the spectroscopic factors for the $1/2^+$ state approach those in a weak-coupling situation due to extending-out of the amplitudes from an interaction region.

§ 5. Conclusions

We have investigated the motion of the valence neutron around two α-clusters by the generator coordinate method. We have found out that the wave functions for the ground rotational band are well localized and are just represented in terms of the molecular orbitals in the LCAO approximation. In spite of weak binding of 1.67 MeV from the ^{8}Be$+n$ threshold there exists a stable intrinsic state for the ground rotational band, which is guaranteed mainly by an effect of the Pauli exclusion principle between the valence neutron and the ^{8}Be core with well developed two-α-cluster structure, and is reinforced by an effect of the spin-orbit force. As for the positive parity states, the motion of the valence neutron is weakly bound with the ^{8}Be core and therefore the wave functions spread widely. But the motion is distorted near a nuclear surface by the effect of the Pauli principle, and the wave functions of the valence neutron have two-center-like distributions as those in the LCAO approximation. As a whole, the positive parity states have intermediate character between the weak- and strong-coupling limit. Above all the first $5/2^+$ and $9/2^+$ states are close to the limit of the LCAO approximation by the effect of the spin-orbit force.

The present investigation reproduces an energy spectrum, an r.m.s.-radius and a quadrupole moment of the ground state and charge form factors to members of the ground rotational band, as well as the previous investigation with the LCAO approximation did. Moreover it reproduces a binding energy from the ^{8}Be$+n$ threshold. We have many quasi-bound states at high excitation energies due to the bound state approximation. In order to examine whether they actually exist or not we are now investigating them under a scattering boundary condition. Among the quasi-bound states the third $3/2^+$ state has a large overlapping on the state in the LCAO approximation and is a parity inverted state of the ground $3/2^-$ state and may be a candidate for the Pygmy resonance in a photo-neutron reaction.

The charge form factors to the positive partity states which have never been

explained are now reproduced excellently well. We have found out that small components not included in the truncated space of the LCAO approximation, especially in the $1/2^+$ state at 1.68 MeV, determine the dependence of the charge form factors on transfer momenta, and that improvement of tail parts of wave functions of the valence neutron makes calculated values of the form factors large so as to fit the experiments. The improved behaviors of the wave functions have been clearly seen in neutron reduced width amplitudes.

The present investigation predicts the $1/2^-$ rotational band as well as the previous paper, while there is no experimental indication on the states except the $1/2^-$ state at 2.78 MeV. The experimental measurements on the states, for example, magnetic form factors for electron scattering, are strongly desired.

We conclude that we have unifiedly understood the properties of the ^{9}Be nucleus at low energies, those of the negative and positive partity states, based on the $2\alpha+n$ molecular structure.

Acknowledgements

The authors would like to express their thanks to Professor H. Tanaka for useful discussions. They also thank the other members of the Nuclear Laboratory of Hokkaido University for their encouragements. This work was performed as a part of the annual research on the "Alpha-like Four-Body Correlations and the Molecular Structure in Light Nuclei" in 1977 and 1978 organized by the Research Institute for Fundamental Physics, Kyoto University, Kyoto. The authors were indebted to the Grant-in-aid for Scientific Research of Ministry of Education, Science and Culture under the special project on Heavy Ion Science. The numerical calculations were carried out on FACOM 230-75 at Hokkaido University Computing Center and on HITAC 8800/8700 at Computer Center of University of Tokyo.

References

1) See for example, Prog. Theor. Phys. Suppl. No. 52 (1972), Prog. Theor. Phys. Suppl. No. 62 (1978). *Proceedings of the 3rd International Conference on Clustering Aspects of Nuclear Structure and Nuclear Reactions, Manitoba* (1978).
2) Y. Abe, J. Hiura and H. Tanaka, Prog. Theor. Phys. **49** (1973), 800.
3) S. Okabe, Y. Abe and H. Tanaka, Prog. Theor. Phys. **57** (1977), 866.
4) S. Okabe and Y. Abe, Prog. Theor. Phys. **59** (1978), 315.
5) S. Okabe, *Proceedings of the International Conference on Nuclear Structure* (*Contributed papers*), Tokyo (1977), p. 154.
6) F. C. Barker, Nucl. Phys. **28** (1961), 96.
L. Grünbaum and M. Tomaselli, Nucl. Phys. **A160** (1971), 437.
7) F. Ajzenberg-Selove and T. Lauritsen, Nucl. Phys. **A227** (1974), 1.
8) W. Zahn, Nucl. Phys. **A269** (1976), 138.
9) D. L. Hill and J. A. Wheeler, Phys. Rev. **89** (1953), 1106.
D. M. Brink, *International School of Physics "Enrico Fermi", XXXVI* (1966), 247.
10) R. A. Arndt, D. D. Long and L. D. Roper, Nucl. Phys. **A209** (1973), 429.

R. A. Arndt and L. D. Roper, Nucl. Phys. **A209** (1973), 447.
11) N. P. Heydenberg and G. M. Temmer, Phys. Rev. **104** (1956), 123.
R. Nilson, W. K. Jentschke, G. R. Briggs, R. O. Kerman and J. N. Snyder, Phys. Rev. **109** (1958), 850.
T. A. Tombrello and L. S. Senhouse, Phys. Rev. **129** (1963), 2252.
12) A. B. Volkov, Nucl. Phys. **74** (1965), 33.
13) S. Nagata, private communication.
14) A. Hasegawa and S. Nagata, Prog. Theor. Phys. **45** (1971), 1786.
15) Y. Mito and M. Kamimura, Prog. Theor. Phys. **56** (1976), 583.
M. Kamimura, Prog. Theor. Phys. Suppl. No. 62 (1978), 236.
16) R. Nathans and J. Halpern, Phys. Rev. **92** (1953), 940.
T. Aurdal, Z. Naturforsch. **24a** (1969), 1188.
17) U. Meyer-Berkhout, K. W. Ford and A. E. S. Green, Ann. of Phys. 8 (1959), 119.
18) M. Bernheim, T. Stovall and D. Vinciguerra, Nucl. Phys. **A97** (1967), 488.
19) M. Bernheim, R. Riskalla, T. Stovall and D. Vinciguerra, Phys. Letters **30B** (1969), 412.
20) H. Nguyen Ngoc, M. Hors and J. P. Y. Jorba, Nucl. Phys. **42** (1963), 62.
21) A. G. Slight, T. E. Drake and G. R. Bishop, Nucl. Phys. **A**208 (1973), 157.
22) H.-G. Clerc, K. J. Wetzel and E. Spamer, Nucl. Phys. **A120** (1968), 441.